Drag power kite with very high lift coefficient

Bauer, F.; Kennel, R.M.; Hackl, C.M.; Campagnolo, F.; Patt, M.; Schmehl, Roland

DOI
10.1016/j.renene.2017.10.073

Publication date
2018

Document Version
Final published version

Published in
Renewable Energy

Citation (APA)
Bauer, F., Kennel, R. M., Hackl, C. M., Campagnolo, F., Patt, M., & Schmehl, R. (2018). Drag power kite with very high lift coefficient. *Renewable Energy*, *118*, 290-305. https://doi.org/10.1016/j.renene.2017.10.073

Renewable Energy 118 (2018) 290–305

Contents lists available at ScienceDirect

Renewable Energy

journal homepage: www.elsevier.com/locate/renene

Drag power kite with very high lift coefficient

Florian Bauer [a, *], Ralph M. Kennel [a], Christoph M. Hackl [b], Filippo Campagnolo [c], Michael Patt [d], Roland Schmehl [e]

[a] Institute for Electrical Drive Systems and Power Electronics, Technical University of Munich, Arcisstrasse 21, 80333 Munich, Germany
[b] Research Group "Control of Renewable Energy Systems", Munich School of Engineering, Lichtenbergstraße 4a, 85748 Garching, Germany
[c] Chair of Wind Energy, Technical University of Munich, Boltzmannstrasse 15, 85748 Garching, Germany
[d] Hochschule Kempten, University of Applied Sciences, Bahnhofstrasse 61, 87435 Kempten, Germany
[e] "Kite Power" Research Group, Aerospace Engineering Faculty at Deft University of Technology, Kluyverweg 1, 2629 HS Delft, The Netherlands

ARTICLE INFO

Article history:
Received 12 April 2017
Received in revised form
31 August 2017
Accepted 23 October 2017
Available online 31 October 2017
2010 MSC
65Z05

Keywords:
Crosswind kite power
Drag power
Airborne wind turbine
High-lift airfoil
Biplane
Genetic algorithm

ABSTRACT

As an alternative to conventional wind turbines, this study considered kites with onboard wind turbines driven by a high airspeed due to crosswind flight ("drag power"). The hypothesis of this study was, that if the kite's lift coefficient is maximized, then the power, energy yield, allowed costs and profit margin are also maximized. This hypothesis was confirmed based on a kite power system model extended from Loyd's model. The performance of small-scale and utility-scale kites in monoplane and biplane configurations were examined for increasing lift coefficients. Moreover, several parameters of the utility-scale system were optimized with a genetic algorithm. With an optimal lift coefficient of 4.5, the biplane outperformed the monoplane. A 40 m wing span kite was expected to achieve a rated power of about 4.1 MW with a power density of about 52 kW/m^2. A parameter sensitivity analysis of the optimized design was performed. Moreover, to demonstrate the feasibility of very high lift coefficients and the validity of a utilized simplified airfoil polar model, CFDs of a proposed high-lift multi-element airfoil were performed and the airfoil polars were recorded. Finally, a planform design of a biplane kite was proposed.

1. Motivation

Kites are tethered wings and promising alternatives to harvest wind energy (cf. e.g. Refs. [1–4]). As shown in Fig. 1, a kite is flown in crosswind trajectories like figure eights or circles.

The considered kite has onboard turbines and generators to generate electrical power which is transmitted to the ground via electrical cables integrated in the tether [5]. Due to the high speed of the kite, the (true) airspeed at the kite is about a magnitude higher than the actual wind speed, so that the onboard turbines are small. For vertical take-off and subsequent transition into crosswind flight, the generators and wind turbines are used as motors and propellers. The reverse procedure is used for the landing when the wind calms down or for maintenance. This airborne wind energy concept is called "crosswind kite power/drag power" [1], or sometimes also "onboard-", "continuous power generation", "fly-gen" or "airborne wind turbine".

Compared to conventional wind turbines, crosswind kite power promises to harvest wind energy at higher altitudes with stronger and steadier winds, but by requiring only a fraction of the material. Hence, it promises to have lower capital costs and in the end a lower levelized cost of electricity (LCOE) or/and higher profits (cf. e.g. Refs. [1–4]). A drag power kite with a rated power of 20 kW ("Wing 7") was developed by the company Makani Power/Google and demonstrated autonomously power generation as well as launching and landing [6,7]. Currently, a full-scale 600 kW system ("M600") is being developed [6–8].

The kite power plant development is a difficult, interdisciplinary challenge. Many studies investigate the modeling, control and flight path optimization (e.g. Ref. [9]), but only a few studies investigate how the kite design can be optimized, and, if so, mainly focus on the tether length and flight altitude (e.g. Ref. [10]). Moreover, most previous studies consider an airfoil of the main wing with a rather low lift coefficient of around one or two (cf. e.g. Refs. [2,9–11]): A study which focused on the kite's airfoil is e.g. Ref. [12], in which an airfoil for kite power applications was optimized, but the usually significant tether drag was neglected and

* Corresponding author.
E-mail address: florian.bauer@tum.de (F. Bauer).

https://doi.org/10.1016/j.renene.2017.10.073
0960-1481/

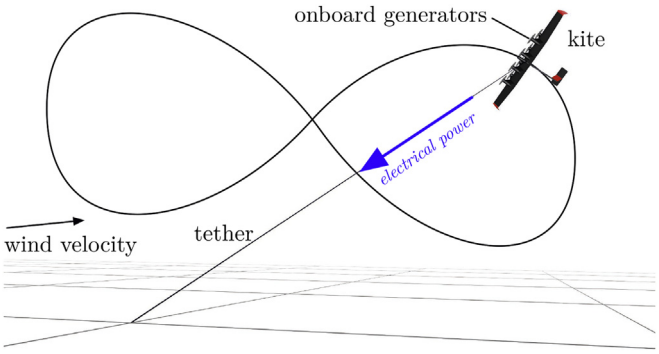

Fig. 1. Illustration of "drag power".

only a single element airfoil with a lift coefficient below two was considered. A study which focused on the kite design is e.g. Ref. [13], but also only a single element airfoil with a relatively low lift coefficient was considered, although the authors concluded: "It turns out that $C_{L,max}$ of the wing is the driving coefficient to design for." Some works investigated and optimized the economic performance (cf. e.g. Ref. [14], [2, Chap. 3], [2, Chap. 15], [15]), but focused on another crosswind kite power concept called "lift power" and, most importantly, also considered only a low lift coefficient of 1.5 or below. Only very recently the patent [16] filed by Makani Power/Google was published in which a two-element airfoil with a maximum lift coefficient of up to four is disclosed, but different possible ranges of maximum lift coefficients and only little details are given for the specific choice of the lift coefficient.—It is important to notice, that the power P of a drag power kite of a given size and at a given wind speed is proportional to

$$P \sim \frac{C_L^3}{C_{D,eq}^2} \tag{1}$$

where C_L is the effective (system) lift coefficient and $C_{D,eq}$ is the effective (system) equivalent drag coefficient, which includes the drag of the kite *and* the drag of the tether (cf. [1,2,17], or Sect. 2 below). In many publications (e.g. Ref. [17]), Eq. (1) is written as

$$P \sim E_{eq}^2 C_L \tag{2}$$

where $E_{eq} = C_L/C_{D,eq}$ is the *effective* (system) glide ratio (which includes the drag of the tether), which falsely suggests that a maximization of the glide ratio of the main wing's *airfoil* maximizes the power while the actual value of C_L has little influence.

Because the power increases cubically with C_L and decreases only quadratically with $C_{D,eq}$, moreover whose major contributor usually is the tether drag, the following Hypothesis was made in this study:

Hypothesis. *Maximizing the main wing's airfoil lift coefficient to or close to its physically feasible maximum, also maximizes the power and energy yield as well as the allowed costs and profit margin of a drag power kite.*

This Hypothesis was assumed to hold true, even-though a high C_L comes at the cost of a higher $C_{D,eq}$ due to increased parasitic drag, increased induced drag due to increased lift, as well as increased tether drag due to the higher required load capability. To achieve a (very) high C_L, multi-element airfoils were considered, a solution commonly used in commercial airliners for decades through slats and flaps [18].

The contributions of this study can be summarized as follows: (i) formulation/derivation of an extended massless drag power kite model, (ii) rearrangement of the model for fast performance computations solely based on explicit analytical equations which also include economic performance estimations, (iii) numerical performance computations of four kite variants, (iv) optimization of a utility-scale kite design with a genetic algorithm, (v) sensitivity analysis of the optimization, (vi) proof of the study's Hypothesis through (iii)–(v), (vii) proposal and CFD analysis of an airfoil which achieves very high lift coefficients, and (viii) proposal of a new optimal and cost-efficient utility-scale kite design.

This study is organized as follows: The next section derives a mathematical model of the kite and formulates the kite design problem. Sect. 3 rearranges the model into a sequence of explicit analytical equations. Moreover, the performance of four example kite power plants w.r.t. the lift coefficient, a numerical plant optimization also with a parameter sensitivity analysis, a proposed high-lift airfoil and a possible planform kite design are presented. Finally, Sect. 4 gives conclusions and an outlook.

2. Problem description

The potential of crosswind kite power was first explored by Loyd in Ref. [1]. In the following, Loyd's derivation is extended. Parts of the derivation of the kite kinematics and power can also be found in a similar way e.g. in Refs. [1,2] and references therein.

2.1. Kite kinematics and power

The kite kinematics model is based on the following three assumptions:

Assumption 1. *Gravitational and inertial forces are small compared to aerodynamic forces.*

Assumption 2. *The tether is straight, so that, in combination with Assumption 1, aerodynamic force F_a and tether force F_{te} are in balance, i.e. $F_{te} = F_a$, see Fig. 2.*

Assumption 3. *The kite does not fly through its own wake (or the kite's influence on the atmospheric airmass is negligible).*

Assumptions 1–2 can be considered valid for crosswind flight and airspeeds above some minimum (cf. e.g. Ref. [19]). Assumption 3 is usually also valid, as the kite's flight path swept area is large (cf. simulation and experimental results of [2, Chap. 28]).

Fig. 2 (a) shows a kite flying perpendicular to the wind (i.e. crosswind) when the kite is exactly in the downwind position and the aerodynamic force and the tether force are in balance (the sum of these forces is zero due to Assumptions 1–2). Fig. 2 (b) shows the same situation, but tether and wind velocity have azimuth $\varphi \neq 0$. Fig. 2 (c) also shows the same situation from the side with an elevation of $\vartheta \neq 0$. For arbitrary φ and ϑ, one can find the relation

$$\frac{\cos(\varphi)\cos(\vartheta)v_w}{v_a} = \sin(a) = \frac{F_{D,\Sigma}}{F_a}, \tag{3}$$

where v_w is the wind speed, v_a is the (true) airspeed, a can be defined as glide angle[1] and $F_{D,\Sigma}$ is the sum of the drag forces. The aerodynamic forces are determined by

[1] This glide angle is defined in analogy to conventional aircraft glide. Note that the glide angle a is only equal to the angle of attack α if the kite's pitch angle, i.e. the angle between the kite's reference chord line and a line perpendicular to the tether, is zero.

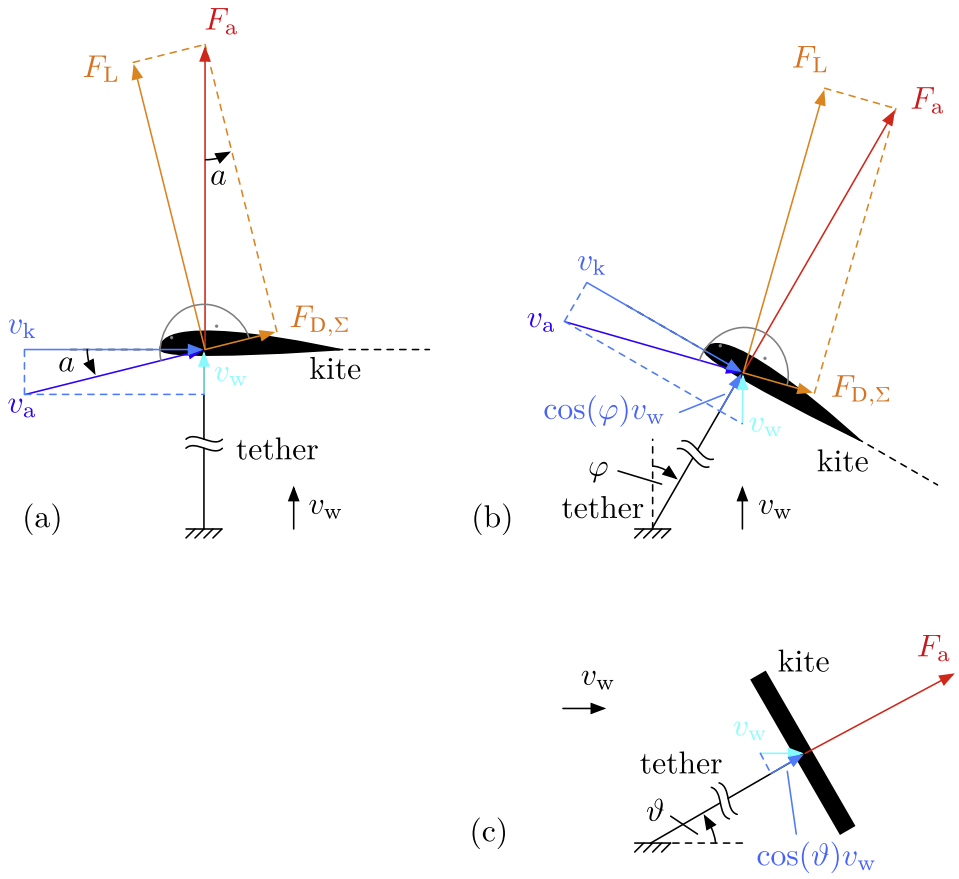

Fig. 2. Sketch of a crosswind flying kite (a) from top, (b) with azimuth angle $\varphi \neq 0$, and (c) seen from the side with elevation angle $\vartheta \neq 0$ while $\varphi = 0$.

$$F_L = \frac{1}{2}\rho v_a^2 A C_L \tag{4}$$

$$F_{D,\Sigma} = \frac{1}{2}\rho v_a^2 A C_{D,\Sigma} \tag{5}$$

$$F_a = \sqrt{F_L^2 + F_{D,\Sigma}^2} \tag{6}$$

with air density ρ, the kite's characteristic (projected wing-) area A, effective lift coefficient C_L and drag coefficient sum $C_{D,\Sigma}$. The latter is given by

$$C_{D,\Sigma} = \underbrace{C_{D,k} + C_{D,te}}_{=: C_{D,eq}} + C_{D,tu} \tag{7}$$

with the kite's effective drag coefficient $C_{D,k}$, the tether drag contribution $C_{D,te}$ (i.e. the contribution of the aerodynamic drag of the tether lumped to the kite), which both can be summarized by an equivalent drag coefficient

$$C_{D,eq} = C_{D,k} + C_{D,te}, \tag{8}$$

and the "drag" coefficient of onboard turbines $C_{D,tu}$ (which is not to be confused with the wind turbine thrust coefficient). Inserting (4)–(6) into (3) and solving for v_a leads to

$$v_a = \cos(\varphi)\cos(\vartheta) v_w \frac{\sqrt{C_L^2 + C_{D,\Sigma}^2}}{C_{D,\Sigma}}. \tag{9}$$

With the turbines' thrust force

$$F_{tu} = \frac{1}{2}\rho v_a^2 A C_{D,tu}, \tag{10}$$

the extracted power by the turbines is given by

$$P_a = v_a F_{tu} \tag{11}$$

$$= \frac{1}{2}\rho \cos^3(\varphi)\cos^3(\vartheta) v_w^3 A \frac{\sqrt{C_L^2 + (C_{D,eq} + C_{D,tu})^2}^3}{(C_{D,eq} + C_{D,tu})^3} C_{D,tu}. \tag{12}$$

2.2. Optimal turbine coefficient

A simple analytical maximum of (12) w.r.t. $C_{D,tu}$ can be found with the following assumption [1]:

Assumption 4. *The effective lift coefficient is much higher than the effective drag coefficient sum so that*

$$\sqrt{C_L^2 + C_{D,\Sigma}^2} \approx C_L. \tag{13}$$

This assumption is valid, as efficient airfoils are considered.

The extracted power is maximized if (i.e. the solution of $0 = \mathrm{d}P_\mathrm{a}/\mathrm{d}C_{\mathrm{D,tu}}$ is) [1]

$$C^*_{\mathrm{D,tu}} = \frac{1}{2} C_{\mathrm{D,eq}} \tag{14}$$

for which the extracted power (12) becomes with (13)

$$P^*_\mathrm{a} = \frac{4}{27}\frac{1}{2}\rho \cos^3(\varphi)\cos^3(\vartheta)\, v_\mathrm{w}^3 A \frac{C_\mathrm{L}^3}{C_{\mathrm{D,eq}}^2} \tag{15}$$

which contains the proportionality stated in (1). Hereby

$$\zeta := \frac{4}{27}\cos^3(\varphi)\cos^3(\vartheta)\frac{C_\mathrm{L}^3}{C_{\mathrm{D,eq}}^2} \tag{16}$$

is defined as power harvesting factor.

2.3. Effective lift and drag coefficients

The effective lift and drag coefficients can be further specified: The effective lift coefficient can be written as (cf. e.g. [20, Chap. 8])

$$C_\mathrm{L} = \frac{c_\mathrm{L}}{1 + \frac{2}{\mathit{AR}}} \tag{17}$$

where c_L is the main wing's airfoil (i.e. 2D-) lift coefficient (which is a function of the airfoil geometry, α and Reynolds number *Re*) and

$$\mathit{AR} = \frac{b^2}{A} \tag{18}$$

is the aspect ratio with wing span *b*.

The kite's effective drag coefficient can be written as

$$C_{\mathrm{D,k}} = C_{\mathrm{D,k,p}} + C_{\mathrm{D,k,i}} + C_{\mathrm{D,k,o}} \tag{19}$$

with effective parasitic $C_{\mathrm{D,k,p}}$ and induced drag $C_{\mathrm{D,k,i}}$ of the main wing, and effective drag of other parts $C_{\mathrm{D,k,o}}$ such as empennage or fuselage (w.r.t. the area of the main wing *A*).

The parasitic drag of the main wing is identical to the parasitic drag of the main wing's airfoil c_D (which is a function of the airfoil's geometry, α and *Re*),

$$C_{\mathrm{D,k,p}} = c_\mathrm{D} \tag{20}$$

and the induced drag of the main wing can be written as (cf. e.g. [20, Chap. 8])

$$C_{\mathrm{D,k,i}} = \frac{C_\mathrm{L}^2}{\pi e \mathit{AR}}, \tag{21}$$

where *e* is the Oswald efficiency number (also called span efficiency).

The airfoil drag coefficient can be further specified e.g. by CFD. However, a simple model for fast optimizations is chosen here by imposing the following assumption:

Assumption 5. *The airfoil drag coefficient increases approximately quadratically with the airfoil's lift coefficient (apart from stall), i.e.*

$$c_\mathrm{D} = c_{\mathrm{D},0} + c_{\mathrm{D},2} c_\mathrm{L}^2, \tag{22}$$

where $c_{\mathrm{D},0}$ is the airfoil's drag coefficient at $c_\mathrm{L} = 0$ and $c_{\mathrm{D},2}$ is the drag coefficient slope w.r.t. the lift coefficient squared.

2.4. Tether drag contribution

The tether drag contribution can be derived as follows (cf. [21–23], [17, Chap. 3.4.1, pp. 44]): An infinitesimal segment of the tether generates the infinitesimal drag force

$$\mathrm{d}F_{\mathrm{D,te}} = \frac{1}{2}\rho v_{\mathrm{a},l_\mathrm{te}}^2 c_{\mathrm{D,te}}\, \mathrm{d}A_\mathrm{te} \tag{23}$$

where $v_{\mathrm{a},l_\mathrm{te}}$ is the component of the airspeed normal to the tether at position l_te, $c_{\mathrm{D,te}}$ is the drag coefficient of the tether's cross section shape, and

$$\mathrm{d}A_\mathrm{te} = d_\mathrm{te}\, \mathrm{d}l_\mathrm{te} \tag{24}$$

is the infinitesimal tether frontal area with tether diameter (or thickness) d_te and infinitesimal length $\mathrm{d}l_\mathrm{te}$.

Because of (13), $v_\mathrm{k} \approx v_\mathrm{a} \gg v_\mathrm{w}$ (cf. also Fig. 2) and the airspeed vector is almost normal to the tether almost along the entire tether length. Therefore, the following two assumptions are imposed:

Assumption 6. *The airspeed at tether length position l_te can be approximated by*

$$v_{\mathrm{a},l_\mathrm{te}} \approx \frac{l_\mathrm{te}}{L_\mathrm{te}} v_\mathrm{a} \tag{25}$$

where L_te is the total tether length and v_a is the airspeed at the kite.

Assumption 7. *Aerodynamic loads of the tether contribute mainly to the kite's drag, while loads in other directions are negligible.*

The drag load of the tether (23) is distributed along the tether and thus partly acts on both, the ground station and the kite. Only the latter contributes to the drag of the kite. To derive that, first the moment of the distributed drag (23) w.r.t. the ground station is derived, that is

$$M_{\mathrm{D,te}} = \int_0^{L_\mathrm{te}} l_\mathrm{te} \times \mathrm{d}F_{\mathrm{D,te}}. \tag{26}$$

The same moment, can also be expressed by

$$M_{\mathrm{D,te}} = L_\mathrm{te} \times F_{\mathrm{D,te}} \tag{27}$$

where $F_{\mathrm{D,te}}$ is the tether drag load expressed as concentrated effective force at the kite. By equating (26) with (27), solving for $F_{\mathrm{D,te}}$, inserting (23)–(25) and integrating over the complete tether length, the tether drag force contribution acting at the kite is given by

$$\begin{aligned} F_{\mathrm{D,te}} &= \frac{\int_0^{L_\mathrm{te}} l_\mathrm{te}\mathrm{d}F_{\mathrm{D,te}}}{L_\mathrm{te}} \\ &= \frac{1}{8}\rho v_\mathrm{a}^2 d_\mathrm{te} L_\mathrm{te} c_{\mathrm{D,te}}. \end{aligned} \tag{28}$$

In (5) with (7), the tether drag force at the kite was given w.r.t. the kite area via tether drag contribution $C_{\mathrm{D,te}}$. Equating both tether drag force equations, i.e. (5) with $C_{\mathrm{D,te}}$ and (28), gives $C_{\mathrm{D,te}}$ as function of the tether parameters,

$$\begin{aligned} F_{\mathrm{D,te}} &= \frac{1}{2}\rho v_\mathrm{a}^2 A C_{\mathrm{D,te}} = \frac{1}{8}\rho v_\mathrm{a}^2 d_\mathrm{te} L_\mathrm{te} c_{\mathrm{D,te}} \\ &\Leftrightarrow C_{\mathrm{D,te}} = \frac{1}{4}\frac{d_\mathrm{te} L_\mathrm{te}}{A} c_{\mathrm{D,te}}. \end{aligned} \tag{29}$$

2.5. Required tether diameter

The tether diameter (or thickness) can be designed according to the expected load which, with (13), is approximately equal to the lift force (4), i.e.

$$F_{\mathrm{te,r}} \approx F_{\mathrm{L,r}} = \frac{1}{2}\rho v_{\mathrm{a,r}}^2 A C_{\mathrm{L,r}} \tag{30}$$

where $F_{\mathrm{te,r}}$ is the rated (maximum) tether force, $F_{\mathrm{L,r}}$ is the rated (maximum) lift force, $v_{\mathrm{a,r}} = v_{\mathrm{a,max}}$ is the rated (maximum) airspeed and $C_{\mathrm{L,r}}$ is the rated effective lift coefficient.

With safety factor S_{te} and tether material yield strength σ_{te}, the required tether core area is

$$A_{\mathrm{te,core}} = S_{\mathrm{te}} \frac{F_{\mathrm{te,r}}}{\sigma_{\mathrm{te}}} \tag{31}$$

from which the tether core diameter (considering a circular core) is determined by

$$A_{\mathrm{te,core}} = \pi \frac{d_{\mathrm{te,core}}^2}{4} \quad \Leftrightarrow \quad d_{\mathrm{te,core}} = 2\sqrt{\frac{A_{\mathrm{te,core}}}{\pi}}. \tag{32}$$

As the tether also has electrical cables, possibly communication cables and a jacket (cf. [5]), the tether diameter (or thickness) is larger than the core, which can be modeled by a multiplicative increase factor $f_{\mathrm{te}} \geq 1$ and/or an additive increase term $\Delta_{\mathrm{te}} \geq 0$ given by

$$d_{\mathrm{te}} = d_{\mathrm{te,core}} f_{\mathrm{te}} + \Delta_{\mathrm{te}}. \tag{33}$$

2.6. Rated power

The rated power is given at the rated airspeed $v_{\mathrm{a,r}}$ with optimal turbine coefficient (14) inserted into (10)–(11), i.e.

$$P_{\mathrm{a,r}} = \frac{1}{2}\rho v_{\mathrm{a,r}}^3 A C_{\mathrm{D,tu}}^*. \tag{34}$$

2.7. Minimum tether length

With (13), the airspeed is approximately equal to the kite's speed $v_{\mathrm{k}} \approx v_{\mathrm{a}}$. The kite travels on a sphere with the radius of the tether length L_{te}. The maximum (rated) angular velocity on this sphere is

$$\omega_{\mathrm{max}} = \frac{v_{\mathrm{a,max}}}{L_{\mathrm{te}}}. \tag{35}$$

As the flight direction has to be changed permanently to keep the kite on a figure eight or circular flight path, there is some upper limit for ω_{max}, or by implication a lower limit for L_{te} given by

$$L_{\mathrm{te}} \geq L_{\mathrm{te,min}} = \frac{v_{\mathrm{a,max}}}{\omega_{\mathrm{max}}}. \tag{36}$$

2.8. Minimum airspeed

During crosswind flight, a certain minimum airspeed must hold for Assumptions 1–2 and to keep the kite airborne. To estimate that, Fig. 3 shows a sketch of the kite from the side. It is similar to Fig. 2 (c), but the model does not entirely neglect the gravitational force of the kite which has to be balanced partly by the aerodynamic force. Hereby, $\psi_{\mathrm{w,max}}$ is the maximum roll angle (w.r.t. the tether) to balance the weight. By invoking the law of sines, one finds the trigonometric relation

$$\frac{F_{\mathrm{a}}}{\sin(\vartheta + \pi/2)} = \frac{F_{\mathrm{g}}}{\sin\left(\psi_{\mathrm{w,max}}\right)} \tag{37}$$

where

$$F_{\mathrm{g}} = mg \tag{38}$$

is the gravitational force with effective airborne mass m (which is the kite's mass plus about half of the tether's mass) and gravitational acceleration g. Inserting (38) and (6) into (37) and by invoking (13), the minimum airspeed is given by

$$\begin{aligned} &\frac{\frac{1}{2}\rho v_{\mathrm{a,min}}^2 A C_{\mathrm{L}}}{\cos(\vartheta)} = \frac{mg}{\sin\left(\psi_{\mathrm{w,max}}\right)} \\ \Leftrightarrow &v_{\mathrm{a,min}} = \sqrt{\frac{mg}{\frac{1}{2}\rho A C_{\mathrm{L}}} \frac{\cos(\vartheta)}{\sin\left(\psi_{\mathrm{w,max}}\right)}}. \end{aligned} \tag{39}$$

Apart from estimating $v_{\mathrm{a,min}}$, a negligible roll angle is assumed and thus Assumptions 1–2 are not relaxed in the remainder of this study.

2.9. Wind speed at kite position

The wind speed at the altitude (position) of the kite can be described by the logarithmic wind shear (cf. e.g. [24, Chap. 2.6], [25, Chap. 6.2])

$$v_{\mathrm{w}} = v_{\mathrm{w},h_{\mathrm{ref}}} \frac{\ln\left(\frac{h}{z_0}\right)}{\ln\left(\frac{h_{\mathrm{ref}}}{z_0}\right)} \tag{40}$$

where $v_{\mathrm{w},h_{\mathrm{ref}}}$ is the wind speed in the reference altitude h_{ref},

$$h = L_{\mathrm{te}} \sin(\vartheta) \tag{41}$$

is the altitude of the kite and z_0 is the roughness length.

The probability of a certain wind speed in the reference altitude can be described by the Rayleigh distribution (cf. e.g. [24, Chap. 2.4], [25, Chap. 6.2])

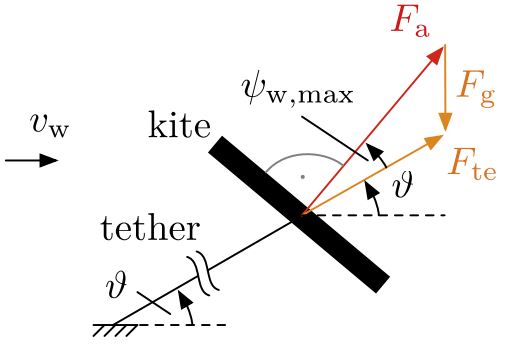

Fig. 3. Sketch of a crosswind flying kite with gravity, seen from the side.

$$p\left(v_{w,h_{ref}}\right) = \frac{\pi}{2}\frac{v_{w,h_{ref}}}{\tilde{v}^2_{w,h_{ref}}}\exp\left(-\frac{\pi}{4}\frac{v^2_{w,h_{ref}}}{\tilde{v}^2_{w,h_{ref}}}\right) \tag{42}$$

where $\tilde{v}_{w,h_{ref}}$ is the mean wind speed in the reference altitude.

2.10. Efficiency and electrical power

The power extracted by the wind turbines is transformed into mechanical power of the turbine shafts and is further transformed into different kinds of electrical power (e.g. AC-DC-AC, cf. [5]) before it is fed into the grid. The electrical power fed into the grid, or demanded from the grid in case the turbines are used as propellers, can be modeled by

$$P_{el} = \begin{cases} \eta P_a & \text{for } P_a \geq 0 \text{ (kite generates power)} \\ \frac{1}{\eta}P_a & \text{for } P_a < 0 \text{ (kite demands power)} \end{cases} \tag{43}$$

where the efficiency $\eta \leq 1$ accounts for all power conversion losses (which is here considered equal for both power flow directions) between P_a and P_{el}.

Remark 1. *The power extracted by the onboard turbines is limited by Betz' law. However, as the axial induction factors of the wind turbines of a drag power kite are usually small, η can be close to one* (cf. [*2, Chap. 28.2.5*]).

2.11. Power curve

Similar to a conventional wind turbine, the power curve of a drag power kite has four main regions (cf. [2, Chap. 28] and Fig. 5 below in Sect. 3.3):

I: In the first region at low wind speeds $0 \leq v_w \leq v_{w,I\to II}$, the wind is insufficient for optimal power generation. The kite needs to be grounded or propelled by the rotors/propellers (Region I(a)), or a lower than optimal turbine drag coefficient has to be applied (Region I(b)). Consequently, $C_{D,tu} \neq C^*_{D,tu}$ and is instead controlled such that the minimum airspeed $v_{a,min}$ is achieved. The turbine drag coefficient at which $v_{a,min}$ is achieved as function of the wind speed is, with (7) in (9) and by invoking (13), given by

$$\begin{aligned} v_{a,min} &= \cos(\varphi)\cos(\vartheta)\, v_w \frac{C_L}{C_{D,\Sigma}} \\ &= \cos(\varphi)\cos(\vartheta)\, v_w \frac{C_L}{C_{D,eq} + C_{D,tu}} \\ \Leftrightarrow C_{D,tu} &= \frac{\cos(\varphi)\cos(\vartheta)\, v_w}{v_{a,min}} C_L - C_{D,eq} \end{aligned} \tag{44}$$

with which the power (11) becomes

$$P_{a,I} = \frac{1}{2}\rho A v^3_{a,min}\left(\frac{\cos(\varphi)\cos(\vartheta)\, v_w}{v_{a,min}} C_L - C_{D,eq}\right). \tag{45}$$

It is meaningful to keep the kite grounded at very low wind speeds, at which the power would otherwise be negative, i.e. the wind turbines would be operated as propellers. Moreover, launching and landing maneuvers can be expected short and rare compared to normal or off operation, thus the energy demand for launching and landing can be neglected. Hence, with (43), the generated electrical power in the first region can be written as

$$P_{el,I} = \max\{0, \eta P_{a,I}\}. \tag{46}$$

The wind speed, where the first region ends/the second region starts, can be calculated by inserting $v_a = v_{a,min}$ and $C_{D,tu} = C^*_{D,tu}$ (14) into (9) and solving for v_w, i.e. with (7) and (13) one obtains

$$\begin{aligned} v_{a,min} &= \cos(\varphi)\cos(\vartheta) v_{w,I\to II}\frac{C_L}{C_{D,eq} + C^*_{D,tu}} \\ \Leftrightarrow v_{w,I\to II} &= \frac{v_{a,min}}{\cos(\varphi)\cos(\vartheta)}\frac{\frac{3}{2}C_{D,eq}}{C_L}. \end{aligned} \tag{47}$$

The wind speed at the reference altitude where the first region ends/the second region starts, is given by inserting (47) into (40) and solving for $v_{w,h_{ref}} = v_{w,h_{ref},I\to II}$ which becomes

$$v_{w,h_{ref},I\to II} = v_{w,I\to II}\frac{\ln\left(\frac{h_{ref}}{z_0}\right)}{\ln\left(\frac{h}{z_0}\right)}. \tag{48}$$

Moreover, the cut-in wind speed, which is the wind speed at which the power becomes positive, is given by setting $P_{a,I} = 0$ in (45) and solving for $v_w = v_{w,cut-in}$ which becomes

$$\begin{aligned} 0 &= \frac{1}{2}\rho A v^3_{a,min}\left(\frac{\cos(\varphi)\cos(\vartheta)\, v_{w,cut-in}}{v_{a,min}} C_L - C_{D,eq}\right) \\ \Leftrightarrow v_{w,cut-in} &= \frac{v_{a,min}}{\cos(\varphi)\cos(\vartheta)}\frac{C_{D,eq}}{C_L}. \end{aligned} \tag{49}$$

Note that $v_{w,cut-in} = \frac{2}{3}v_{w,I\to II}$. The cut-in wind speed at reference altitude is given by inserting (49) into (40) and solving for $v_{w,h_{ref}} = v_{w,h_{ref},cut-in}$ which becomes

$$v_{w,h_{ref},cut-in} = v_{w,cut-in}\frac{\ln\left(\frac{h_{ref}}{z_0}\right)}{\ln\left(\frac{h}{z_0}\right)}. \tag{50}$$

II: In the second region at medium wind speeds $v_{w,I\to II} \leq v_w \leq v_{w,II\to III} = v_{w,r}$, no limitations need to be made, so the power is given by (15) and (43), respectively. The rated wind speed at the kite's position is given by inserting $v_{a,r}$ into (9) and solving for $v_w = v_{w,r}$ which, with (7), (13) and (14), becomes

$$v_{w,r} = \frac{v_{a,r}}{\cos(\varphi)\cos(\vartheta)}\frac{\frac{3}{2}C_{D,eq}}{C_L}. \tag{51}$$

Inserting (51) into (40) and solving for $v_{w,h_{ref}} = v_{w,h_{ref},r}$ yields the rated wind speed at reference altitude, i.e.

$$v_{w,h_{ref},r} = v_{w,r}\frac{\ln\left(\frac{h_{ref}}{z_0}\right)}{\ln\left(\frac{h}{z_0}\right)}. \tag{52}$$

III: In the third region at high wind speeds $v_{w,r} = v_{w,II\to III} \le v_w \le v_{w,III\to IV} = v_{w,cut-out}$, the power and the tether force[2] are limited by the flight controller by adjusting c_L, c_D and/or $C_{D,k,o}$ e.g. via flaps/flaperons, angle of attack, angle of sideslip and/or air brakes. Therefore, the power at these wind speeds is constant at the rated power, (34) inserted into (43).
IV: In the forth region at very high wind speeds $v_{w,cut-out} = v_{w,III\to IV} \le v_w$, the wind is too strong for safe operation, so the kite is grounded and no power is generated.

Summarizing, the power curve is given by

$$P_{el}(v_w) = \begin{cases} (46) & \text{for } 0 \le v_w \le v_{w,I\to II} \\ (15)\text{in}(43) & \text{for } v_{w,I\to II} \le v_w \le v_{w,II\to III} \\ (34)\text{in}(43) & \text{for } v_{w,II\to III} \le v_w \le v_{w,III\to IV} \\ 0 & \text{for } v_{w,III\to IV} \le v_w. \end{cases} \tag{53}$$

2.12. Energy yield and capacity factor

With the power curve, the electrical energy yield for one year $E_{el,yr}$ in Wh/yr is given by (cf. e.g. [24, Chap. 3.16,] [25, Chap. 6.7.1])

$$E_{el,yr} = \frac{8,760\text{h}}{1\text{yr}} \cdot \int_0^\infty p\left(v_{w,h_{ref}}\right) P_{el}\left(v_{w,h_{ref}}\right) \mathrm{d}v_{w,h_{ref}} \tag{54}$$

and the capacity factor N is given by (cf. e.g. [26, Chap. 1.6], [27])

$$N = \frac{E_{el,yr} \Big/ \frac{8,760\text{h}}{1\text{yr}}}{P_{el,r}}. \tag{55}$$

2.13. Costs and economic profit

The cost per year k is

$$k = k_{inv} + k_{op} \tag{56}$$

with investment costs k_{inv} and operational costs k_{op}. The investment costs can be written as (cf. e.g. [26, Chap. 1.6], [28])

$$k_{inv} = K_{inv} \frac{I(1+I)^{T/\text{yr}}}{(1+I)^{T/\text{yr}} - 1} \tag{57}$$

where K_{inv} is the total investment price of the power plant, I is the interest rate p.a. (which is expected by the investor of the power plant or the energy utility company) and T is the life time of the power plant (in years). As neither fuel nor pilots or other regular operators are required by a (fully automated) kite power plant, the operational costs per year narrow down, maybe to small costs for a grid operator, checkups or small repairs, if any at all. The operational costs can thus be formulated as a (small) percentage I_{op} of the investment costs p.a.,

$$k_{op} = I_{op} K_{inv}. \tag{58}$$

Inserting (57) and (58) into (56) yields

$$k = K_{inv}\left[I_{op} + \frac{I(1+I)^{T/\text{yr}}}{(1+I)^{T/\text{yr}} - 1}\right]. \tag{59}$$

The investment costs can be further specified by

$$K_{inv} = K_{inv,dt} + K_{inv,o\&p} \tag{60}$$

with

$$K_{inv,dt} = k_{dt} P_{el,r} \tag{61}$$

where $K_{inv,dt}$ is the cost of the drivetrain (i.e. generators and all power electronics), k_{dt} is the specific cost of the drivetrain (in \$/W), and $K_{inv,o\&p}$ is the cost of the airframe, tether, ground station and other parts, includes also development costs, as well as the profit margin of the power plant manufacturer.

The levelized cost of electricity (LCOE) is finally given by (cf. e.g. [26, Chap. 1.6], [28]).

$$k_{LCOE} = \frac{k}{E_{el,yr}}. \tag{62}$$

2.14. Formulation of the kite design problem

The kite design problem can be formulated as follows: Find the optimal kite design parameters (airfoil design i.e. c_L, c_D, wing design b, A, tether length L_{te} and rated airspeed $v_{a,r}$) which minimize a cost function subject to constraints. Finding a suitable cost function and constraints are part of the problem.

3. Proposed kite design optimization approach

For a prototype or product development, one would usually first fix the kite's size, e.g. the span. Moreover, it is near at hand to fix (or limit to a narrow band) the rated/maximum airspeed and thus also the tether length, or vice versa, because the maximum angular velocity is a somewhat fixed value. Additionally, effective elevation and azimuth are fixed or only variable in narrow limits. Consequently, the basic idea is to start with these somewhat fixed parameters for a kite power plant product development and to "inversely" compute and optimize the expected performance:

3.1. Kite performance computation

1. Estimate/fix/select b, ρ, φ,[3] σ_{te}, S_{te}, f_{te}, Δ_{te}, $c_{D,te}$, $C_{D,k,o}$, e, $v_{a,min}$, $\tilde{v}_{w,h_{ref}}$, $v_{w,h_{ref},cut-out}$, z_0, h_{ref}, η, T, I_{op}, I, k_{LCOE} for a projected kite power plant installation.[4]
2. Choose $\mathcal{AR}$, L_{te}, $v_{a,r}$, ϑ.[3] Choose airfoil, i.e. estimate $c_{D,0}$, $c_{D,2}$, c_L.
3. Compute area by solving (18) for A which is

[2] For sake of simplicity, more regions where e.g. only the tether force is limited were not considered in this study.

[3] Azimuth and elevation (and thus altitude and power) actually change consistently as the kite follows a figure eight or circular path. However, effective (constant) values φ and ϑ (and thus h) can be estimated which yield a (constant) power P_a that is identical to the actual average (thus constant) power generated within a full figure eight or circular path.

[4] Generated electricity fed into the power grid is indistinguishable from its power source and arbitrarily useable by any load connected to that power grid. Consequently, the price tag a power plant must achieve is set by the targeted market. Hence the (maximum) allowed investment costs and profit margin of the power plant can be computed, based on environmental and by the investors expected parameters.

$$A = \frac{s^2}{\mathcal{R}}. \tag{63}$$

4. Compute/estimate c_L and c_D for the airfoil with (22) *or through CFDs.*
5. Compute effective lift coefficient (17).
6. Compute tether diameter (30)–(33).
7. Compute equivalent drag coefficient (19)–(21), (29), (8).
8. Compute rated power (43) with (34) and (14). *Optionally compute power harvesting factor* (16).
9. Compute the rated wind speed at the kite's position (51) and at the reference altitude (52) with the kite's altitude (41).
10. Compute the cut-in wind speed at the kite's position (49) and at the reference altitude (50). *Optionally compute the maximum allowed airborne mass $\hat{m}$ by solving (39) for $m = \hat{m}$ which is*

$$\hat{m} = \frac{\frac{1}{2}\rho v_{a,\min}^2 A c_L}{g} \frac{\sin\left(\psi_{w,\max}\right)}{\cos(\vartheta)} \tag{64}$$

11. Compute the power curve for all wind speeds (53) and the year energy yield (54) with (42). *Optionally compute the capacity factor* (55).
12. Compute drivetrain costs (61). Compute *maximum allowed* investment costs $\hat{K}_{inv}$ by solving (56)–(62) for $K_{inv} = \hat{K}_{inv}$ which is

$$\begin{aligned} k &= \hat{K}_{inv}\left[I_{op} + \frac{I(1+I)^T}{(1+I)^T - 1}\right] \\ \Leftrightarrow \hat{K}_{inv} &= \frac{k}{I_{op} + \frac{I(1+I)^T}{(1+I)^T - 1}} \\ &= \frac{k_{LCOE} E_{el,yr}}{I_{op} + \frac{I(1+I)^T}{(1+I)^T - 1}}. \end{aligned} \tag{65}$$

Compute the *maximum allowed* investment costs of airframe etc., development costs and profit margin $\hat{K}_{inv,o\&p}$ by solving (60) for $K_{inv,o\&p} = \hat{K}_{inv,o\&p}$ which is

$$\hat{K}_{inv,o\&p} = \hat{K}_{inv} - K_{inv,dt} \tag{66}$$

(where the result of (65) is to be inserted).

13. If performance is not satisfactory, restart at step 2 with a different set of parameters.

Note that steps 1–12 are explicit, particularly include explicitly the tether sizing, and thus allow for a quick evaluation of a kite design. Step 13 is for an iterative optimization. Note also that the actual airborne mass m and actual costs $K_{\#}$ of the kite power plant may be lower than the computed results of the *maximum allowed* ones, $\hat{m}$ and $\hat{K}_{\#}$, respectively.

3.2. Kite performance as function of lift coefficient

As mentioned in Sect. 1, the Hypothesis was that maximizing the lift coefficient of the airfoil c_L also maximize $P_{el,r}$, $E_{el,yr}$ and $\hat{K}_{inv,o\&p}$ of a kite with given size. In the appendix, the power equation is further elaborated analytically and it is shown, that this hypothesis for the power is true, if tether drag and parasitic drag are dominant.

Moreover, four numerical examples were examined to investigate what the optimal c_L would be: For that, the lift coefficient was increased while all other parameters were kept constant. The considered numerical examples were a small-scale system (or a small off-grid system) and a utility-scale system, both either in monoplane or biplane configuration. Table 1 lists the parameters. The monoplane and biplane configurations were considered with same span and area which implies that the biplane had twice the aspect ratio. For the biplane configuration the wings were considered several chord lengths apart such that their interference was assumed negligible (cf. Sect. 3.5 below). Consequently, a biplane configuration was expected to be more beneficial. Moreover, a biplane design can easier achieve a high-strength low-weight airframe and can easier sustain a high wing loading imposed by a high lift coefficient. For a simple design, rectangular wings (without washout) were considered for all variants. For the wind shear and wind probability distribution, the "reference location" specified in the German renewable energy law was used.

Discussion of results

Fig. 4 visualizes the results for $c_L = 1\ldots6$ (note that such high lift coefficients are feasible, cf. [18]. or Sect. 3.5 below): Parasitic and induced drag coefficients increased with c_L^2, while the tether drag contribution increased with $\sqrt{c_L}$, both as expected (cf. (22), (21) and (32)). As the rated airspeed and the area were unchanged, the increased drag lead to increasing rated power and rated power per area with $\approx c_L^2$, but also to increasing cut-in and rated wind speeds for high c_L. For the small-scale system the power harvesting factor reached its maximum at around $c_L \approx 4$ and for the utility-scale system slightly less, at around $c_L \approx 3$. Moreover, for all variants, the capacity factor and the maximum allowed costs per rated power reached their maximum at rather low lift coefficients around $c_L \approx 1.5\ldots2$. However, energy yield, maximum allowed costs and maximum allowed costs per area had their maximum at $c_L \approx 2.5\ldots3$ for the monoplane and at $c_L \approx 4\ldots5$ for the biplane.

Compared to the biplane, the monoplane had a considerably higher rated power, but due to the higher drag also considerably higher rated wind speed and thus considerably lower power harvesting factor, energy yield, capacity factor and maximum allowed costs. To reduce rated and cut-in wind speed of the monoplane, e.g. $v_{a,r}$ would need to be reduced, which in turn would considerably reduce the rated power. Therefore, the biplane outperformed the monoplane, as expected.

Moreover, the utility-scale systems had considerably lower cut-in and rated wind speeds and considerably higher power per wing area and maximum allowed costs per wing area. This can be explained by the lower tether drag contribution due to the larger kite area (cf. (29)) and the higher Reynolds number (cf. Table 1).

3.3. Optimization

Step 13 of the kite performance computation sequence of Sect. 3.1 can be used to optimize the parameters of step 2 iteratively w.r.t. a cost function and subject to constraints. With Fig. 4 and the discussion of the previous section, the difficulty is to find a suitable figure of merit for the cost function and suitable constraints. The rated power alone is obviously not a good figure of merit, as it can

Table 1
Parameters of four possible kite systems.

Parameter	Small Sys.	Utility Sys.	Comment
b[m]	4	40	chosen fixed
A[m^2]	1	80	chosen fixed
ρ[kg/m^3]	1.2	1.2	$\approx$ standard atmosphere
$C_{\mathrm{D,k,o}}$	0.01	0.01	estimated
e	0.7	0.7	rectangular wing chosen
$c_{\mathrm{D,0}}$	0.0167	0.0100	estimated based on CFDs[a]
$c_{\mathrm{D,2}}$	0.0083	0.0050	estimated based on CFDs[a]
$v_{\mathrm{a,r}}$[m/s]	50	80	chosen fixed
$v_{\mathrm{a,min}}$[m/s]	25	35	estimated requirement[b]
$v_{\mathrm{w},h_{\mathrm{ref}}}$[m/s]	0 … 30	0 … 30	all reasonable wind speeds
$v_{\mathrm{w},h_{\mathrm{ref}},\mathrm{cut-out}}$[m/s]	25	25	chosen fixed/estimated
L_{te}[m]	150	500	chosen fixed
f_{te}	1.5	1.3	estimated
Δ_{te}[m]	0	0	not used
S_{te}	3	3	chosen fixed
σ_{te}[GPa]	3.09	3.09	$\approx\sigma$ for Dyneema
$c_{\mathrm{D,te}}$	1.0	1.0	$\approx c_{\mathrm{D}}$ of cylinder at reasonable Re
ϑ[°]	30	30	estimated
φ[°]	15	15	estimated
z_0	0.1	0.1	reference of German law [30]
h_{ref}[m]	30	30	reference of German law [30]
$\tilde{v}_{\mathrm{w},h_{\mathrm{ref}}}$[m/s]	5.5	5.5	reference of German law [30]
η	0.80	0.80	estimated
T[yr]	20	20	chosen fixed, usual for wind energy
l_{op}[%/yr]	5	5	estimated
I[%/yr]	10	10	chosen fixed/estimated requirement
k_{dt}[$/W]	0.15	0.15	estimated[c]
k_{LCOE}[$/kWh]	0.05	0.05	chosen fixed/estimated requirement
$\mathcal{AR}_{\mathrm{monoplane}}$	16	20	result from (18)
$\mathcal{AR}_{\mathrm{biplane}}$	32	40	result from (18) multiplied by two
h[m]	75	250	result from (41)

[a] Cf. Sect. 3.5/Fig. 8 below. Value for small-scale system was estimated 2/3 higher because of a significantly lower Re.
[b] E.g. with $C_{\mathrm{L}} = 5$, $\psi_{\mathrm{w,max}} = 20^\circ$, $g = 9.81$ m/s^2 and the other parameters of this table inserted into (64), the maximum allowed airborne mass of the small-scale system is $\hat{m} \approx 75$kg and for the utility-scale system $\hat{m} \approx 11,836$kg, which both seem feasible (cf. [29]).
[c] As an example, the "Turnigy RotoMax 100 cc" costs 333.84$ and has a rated power of 7992W [31], hence a specific cost of 0.0418$/W. Assuming that the drive power electronics and ground station power electronics for the grid connection both have the same specific costs, the specific drivetrain cost is the triple 0.1245$/W. As further a high voltage for the tether with high voltage converters, a low weight for kite parts, a high quality and a long lifetime are required, this amount was rounded up to 0.15$/W.

be very high for high drag coefficients but at the cost of a high rated wind speed. The rated power might be a good figure of merit with the constraint of a certain rated wind speed, which however has to be chosen to "some" value. Also the capacity factor ("capacity factor paradox" [32]) or maximum allowed costs per rated power alone do not seem to be suitable figures of merit, as higher energy yields, with which revenue is generated, are achieved off their maxima. A suitable cost function for the electricity customer might be the minimization of k_{LCOE}. For the kite power plant manufacturer, a suitable cost function might be the maximization of the profit margin. However, for both previous variants a detailed model for the actual $K_{\mathrm{inv,o\&p}}$ has to be found, which is out of scope of this study. For an environmental activist, a suitable cost function could be the maximization of $E_{\mathrm{el,yr}}$ as this is the actual contribution for the energy shift with more renewable energy generation. For an energy utility company or the kite power plant investor it might be interesting to maximize the revenue, i.e. $k_{\mathrm{LCOE}}E_{\mathrm{el,yr}}$ (which is the same as maximizing $E_{\mathrm{el,yr}}$ for a fixed k_{LCOE}), as this generates the return on investment. Other values such as the land use might also be objectives, but also require model refinements/extensions which are not in scope of this study. A suitable cost function might also be the minimization/maximization of several figures of merit simultaneously (multi-objective optimization).

Here, as a compromise, the maximum allowed investment costs of airframe etc., development costs and profit margin w.r.t. the wing area was selected as cost function to be maximized with reasonable constraints on the optimization parameters, because (i) the kite power plant manufacturer decides how to design its kite, (ii) it has a high interest in having a high budget for the plant development as well as a high profitability margin, (iii) it can be assumed that the costs of a kite power plant product are dominated by the development costs, particularly in view of today's low technology readiness level, and (iv) the airframe costs can be expected to be (somewhat) proportional to the wing area (at least increase with the wing area). The selected optimization problem can thus be written as

$$\max_{\mathcal{AR},v_{\mathrm{a,r}},L_{\mathrm{te}},\vartheta,c_{\mathrm{L}}} \quad \frac{\hat{K}_{\mathrm{inv,o\&p}}}{A} \tag{67}$$

$$\text{s.t.} \quad \underline{\mathcal{AR}} \leq \mathcal{AR} \leq \overline{\mathcal{AR}} \tag{68}$$

$$\underline{v}_{\mathrm{a,r}} \leq v_{\mathrm{a,r}} \leq \overline{v}_{\mathrm{a,r}} \tag{69}$$

$$L_{\mathrm{te,min}} = \frac{v_{\mathrm{a,r}}}{\omega_{\mathrm{max}}} \leq L_{\mathrm{te}} \leq \overline{L}_{\mathrm{te}} \tag{70}$$

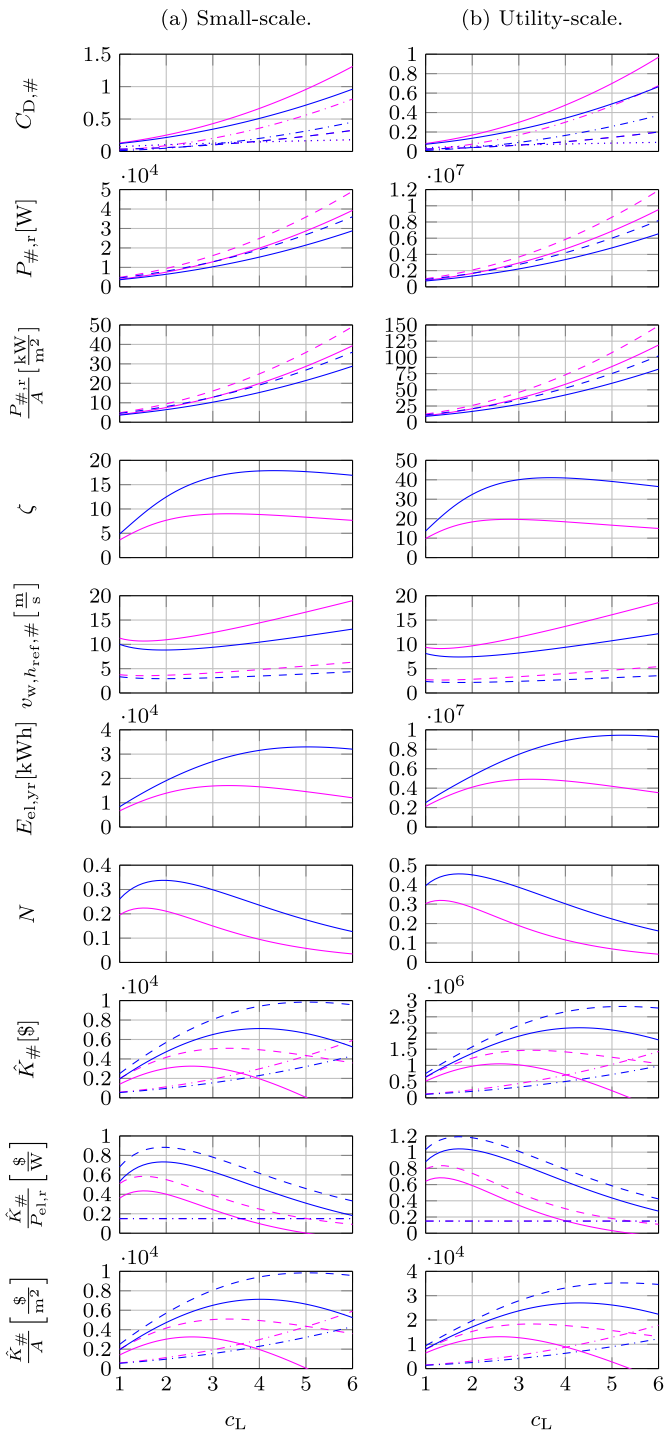

Fig. 4. Performance results as function of c_L (a) for the small-scale system and (b) for the utility-scale system with monoplane configuration in magenta and biplane configuration in blue. From top to bottom: equivalent drag coefficient $C_{D,eq}$ in solid (−), sum of parasitic drag coefficient and drag of other parts $C_{D,k,p} + C_{D,k,o}$ in dashed (- - -), induced drag coefficient $C_{D,k,i}$ in dash-dotted (- · - ·), and tether drag contribution $C_{D,te}$ in dotted (·····); rated extracted power $P_{a,r}$ in dashed (- - -) and rated electrical power $P_{el,r}$ in solid (−); rated extracted power per area $P_{a,r}/A$ in dashed (- - -) and rated electrical power per area $P_{el,r}/A$ in solid (−); power harvesting factor ζ; rated wind speed in reference altitude $v_{w,h_{ref},r}$ in solid (−) and cut-in wind speed in reference altitude $v_{w,h_{ref},cut-in}$ in dashed (- - -); electrical energy yield for one year $E_{el,yr}$; capacity factor N. The bottom three plots show the maximum allowed investment costs $\hat{K}_{inv,\#}$ absolute, per rated electrical power $P_{el,r}$ and per kite area A, whereby drivetrain costs $K_{inv,dt}$ in dash-dotted (- · - ·), maximum allowed investment costs $\hat{K}_{inv}$ in dashed (- - -), maximum allowed investment costs of airframe etc., development costs and profit margin $\hat{K}_{inv,o\&p}$ in solid (−). (For interpretation of the references to colour in this figure legend, the reader is referred to the web version of this article.)

$$\arcsin\frac{\underline{h}}{L_{te}} \le \vartheta \le \arcsin\frac{\overline{h}}{L_{te}} \tag{71}$$

$$\underline{c}_L \le c_L \le \overline{c}_L, \tag{72}$$

where $\underline{x}$ and $\overline{x}$ are bounds of the respective optimization variable x.

As an example, the optimization of the utility-scale biplane with the parameters in Table 1 and the bounds of the optimization variables in Table 2 was optimized. The Covariance Matrix Adaptation Evolution Strategy (CMA-ES) was used for this task, because the cost function with the few explicit analytical equations of steps 3–12 of Sect. 3.1 can be computed very fast, this algorithm does not require a Jacobean and likely finds the global optimum (cf. e.g. Ref. [33]). Table 3 reports the results of the optimization and Fig. 5 shows the power curve. The computation on a modern computer took only a few seconds with several thousand cost function evaluations.

Discussion of results

Optimal aspect ratio and rated airspeed were at their upper bound. The optimal lift coefficient was with ≈4.5 rather high. The optimal tether length and elevation angle were relatively small, and thus the operation altitude was also relatively low, but higher than today's conventional wind turbine hub heights. This can be explained by the high tether drag penalty for a longer tether and a lower cosine efficiency $\cos(\vartheta)^3$ for higher elevation angles (cf. (15), [34]). The resulting rated electrical power was with ≈4.1MW for such a small kite rather high (the span was only ≈20% of the span of three blades of a conventional wind turbine with similar power rating). This lead to a power density of ≈52kW/m², which was e.g. >250 times denser than photovoltaics. The capacity factor was similar to conventional (onshore) wind turbines, but a considerable increase could be expected for an offshore site (similar to conventional wind turbines, cf. also sensitivity analysis in the next Section 3.4).

It was interesting to execute the optimization also for the monoplane configuration: With similar optimal parameters—including optimal $c_L \approx 4.59$, but area only $A = 40\text{m}^2$ due to $\overline{\mathcal{AR}}$ and a fixed b—, the resulting maximum allowed cost was with $\hat{K}_{inv,o\&p}/A = 25,958.22\$/\text{m}^2$ more than a tenth lower. Moreover, the rated power was only $P_{el,r} \approx 1.79\text{MW}$, which was less than half of the rated power for the biplane. Thus, the biplane outperformed the monoplane again.

For the optimal biplane, $\mathcal{AR}$ and $v_{a,r}$ were at the upper bound. It was also interesting to investigate what the optimum would be, if these bounds are increased. First, the upper bound for the rated airspeed was changed to $\overline{v}_{a,r} = 100\text{m/s}$. The optimal rated airspeed was then with $v_{a,r} = 80.58\text{m/s}$ only slightly higher than before and thus the other design parameters and resulting figures of merit hardly changed. Second, additionally the upper bound of the aspect ratio was changed to $\overline{\mathcal{AR}} = 60$ (which, however, seems unrealistically high). With that, the optimal aspect ratio was at this new upper bound and the optimal lift coefficient increased to $c_L = 5.43$ while the other design parameters changed only slightly. The maximum allowed costs increased significantly to $\hat{K}_{inv,o\&p}/A = 38,342.36\$/\text{m}^2$. These results emphasize the importance, that the kite should have a lift coefficient and an aspect ratio close to or at the attainable maximum.

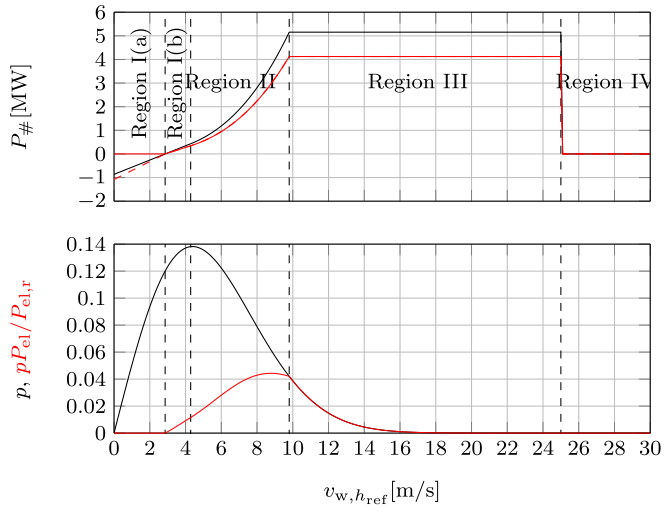

Fig. 5. Power curve of the optimized utility-scale biplane with extracted power P_{a} in (–) and electrical power P_{el} in (——) (top), and wind probability distribution p in (–) and normalized energy yield distribution $pP_{\mathrm{el}}/P_{\mathrm{el,r}}$ in (——) (bottom).

3.4. Parameter sensitivity analysis

As the optimization was based on assumed parameters of step 1 in Sect. 3.1, a sensitivity analysis for the optimal design parameters was required: With individually varied values of (some important) parameters of step 1, the optimization procedure of the last section 3.3 was executed again. Fig. 6 (a)–(f) shows the optimized design parameters of step 2 and Fig. 6 (g)–(l) shows the resulting figures of merit.

Discussion of results

The most important graphs for this study are in Fig. 6 (e): Only for significantly lower e (——) and $\tilde{v}_{\mathrm{w},h_{\mathrm{ref}}}$ (- - -), the optimal c_{L} was significantly lower, but still above 3.5 for the investigated values. However, the baseline e and $\tilde{v}_{\mathrm{w},h_{\mathrm{ref}}}$ were already relatively low so that such a reduction is unlikely. Therefore, the Hypothesis for this study can be confirmed again.

The other graphs of Fig. 6 are also interesting: E.g. the optimized $\mathcal{AR}$, $v_{\mathrm{a,r}}$ and ϑ (Fig. 6 (a), (b), (d)) had almost no sensitivity on any of the investigated parameters, while the optimized L_{te} and thus h (Fig. 6 (c) and (f)) significantly increased for lower f_{te} (——) and higher $\tilde{v}_{\mathrm{w},h_{\mathrm{ref}}}$ (- - -). The latter can be explained by a lower tether drag for lower f_{te} and increased wind speed (and its cubed value, cf. (15)) at higher altitudes for higher $\tilde{v}_{\mathrm{w},h_{\mathrm{ref}}}$. Note that a lower tether drag per tether length through a lower f_{te} was used by the optimizer to increase the tether length to tap higher wind speeds, by which the total tether drag contribution hardly changed. However, this had only limited impact on the figures of merit, cf. (——) in Fig. 6 (g)–(l).

The sensitivity of φ (–) on all optimized design parameters and figures of merit was rather low, which implies that the chosen/feasible flight path (e.g. width of the figure eight) has little influence on the system performance. Moreover, the sensitivity of $c_{\mathrm{D},2}$ (——) on the figures of merit was relatively low.

The sensitivity of $v_{\mathrm{a,min}}$ (——) was high for the cut-in wind speed, but was almost zero for all other figures, which can be explained by the fact that at very low wind speeds also only very low power can be harvested. This implies that the airborne mass has little influence on the performance.

The sensitivity of $\tilde{v}_{\mathrm{w},h_{\mathrm{ref}}}$ (- - -) was rather high for many figures, particularly for the year energy yield and maximum allowed costs (per wing area): e.g. a 40% increase, which can be expected for an offshore site, more than doubled these two figures of merit, but required also a significantly higher lift coefficient up to the bound $c_{\mathrm{L}} = \bar{c}_{\mathrm{L}} = 6$. This high sensitivity is not surprising, as the power increases with the cube of the wind speed—similar to conventional wind turbines. Hence, to obtain optimal design parameters and good estimates of the figures of merits for a power plant deployment, a good estimate for $\tilde{v}_{\mathrm{w},h_{\mathrm{ref}}}$ for the anticipated deployment site is required.

As expected, the sensitivity of η (- - ·) had a linear influence only on the rated electrical power, energy yield and maximum allowed costs.

The sensitivity of I_{op} (- - ·) only had an influence on the maximum allowed costs, but was rather low.

The sensitivity of k_{LCOE} (- - ·) almost only had an influence on the maximum allowed costs, but was rather high: E.g. an increase of k_{LCOE} by 40% to $k_{\mathrm{LCOE}} = 0.07\$/\mathrm{kWh}$ increased the maximum allowed costs by ≈50%. As a consequence, an off-grid system for mines or islands, where the LCOE can be considerably higher, the costs and the profit margin of the kite power plant manufacturer are allowed to be rather high. As the development of the kite power technology is still immature and thus has high development costs, some kite power startups target such markets first.

Table 2
Bounds for the optimization of the utility-scale biplane.

Parameter/ Bound	Value	Comment
$\underline{\mathcal{AR}}$	10	estimated meaningful limit
$\overline{\mathcal{AR}}$	40	estimated feasible limit
$\underline{v}_{\mathrm{a,r}}$[m]	60	estimated meaningful limit
$\bar{v}_{\mathrm{a,r}}$[m]	80	estimated required limit[a]
ω_{max}[°/s]	20	estimated required limit
$\underline{L}_{\mathrm{te}}$[m]	2,000	estimated meaningful limit
$\underline{h}$[m]	100	estimated required limit for safe operation
$\bar{h}$[m]	1,000	estimated required limit to not interfere with aircraft
$\underline{c}_{\mathrm{L}}$	1	estimated meaningful limit
$\bar{c}_{\mathrm{L}}$	6	estimated feasible limit

[a] This is similar to the maximum tip speed of usual conventional wind turbines, although a kite power plant deployed with enough distance to houses particularly offshore or in a desert might allow for higher noise emissions due to an airspeed above that limit.

3.5. CFD of very high-lift multi-element airfoil

For decades commercial airliners can achieve lift coefficients of up to ≈4.5 for airfoils with slats and flaps (cf. e.g. Ref. [18]), despite the design constraints of e.g. retractable slats and flaps for efficient transonic flight with rather low lift and drag coefficients. The airfoil design challenge for a kite is very different compared to a commercial airliner: The lift of a wing portion needs to be controlled with control surfaces to control both the power output and flight path of the kite (e.g. by rolling), but the kite is never flown transonic, the tether drag is a major drag contributor, and the lift is only reduced to limit e.g. power, tether force and airspeed which even benefits if the drag coefficient does not reduce much for reduced lift coefficients. As a conclusion, also with the results of the previous sections, a very high-lift multi-element airfoil, with a high number of elements, wherein one or more airfoil elements at the trailing edge are used as flaperons, appears to be the optimal choice for the airfoil of the main wing(s) of a power generating kite. With that

Table 3
Results of the optimization of the utility-scale biplane.

Parameter	Value
$\mathcal{AR}$	40.00
$v_{a,r}$[m/s]	80.00
L_{te}[m]	539.99
ϑ[°]	20.06
c_L	4.51
A[m^2]	80.00
h[m]	185.20
Figure of Merit	**Value**
$C_{D,k,p} + C_{D,k,o}$	0.12
$C_{D,k,i}$	0.21
$C_{D,te}$	0.09
$C_{D,eq}$	0.42
$P_{el,r}$[MW]	4.12
$P_{el,r}/A$[kW/m^2]	51.55
ζ	49.71
$v_{w,h_{ref},r}$[m/s]	9.80
$v_{w,h_{ref},cut-in}$[m/s]	2.86
$E_{el,yr}$[Mio. kWh]	9.97
N	0.28
$\hat{K}_{inv}$[Mio. $]	2.98
$\hat{K}_{inv,o\&p}$[Mio. $]	2.36
$\hat{K}_{inv,o\&p}/A$[$/m^2]	29,473.89

philosophy, an airfoil was designed which is able to achieve very high maximum lift coefficients of $c_{L,max} > 5$. The airfoil was designed mainly through trail and error, but some parameters such as the distance between the elements and their angles were optimized with CMA-ES. Fig. 7 (top) shows the designed four-element airfoil at the design angle of incidence and Fig. 7 (bottom) shows the same airfoil for a biplane configuration (i.e. the aerodynamic interference of the two wings was not neglected). Fig. 8 compares the lift and drag coefficients.

The CFD was set up in COMSOL Multiphysics and solved by a Reynolds Averaged Navier Stokes (RANS)-solver with the $k\omega$-turbulence model [35]. The $k\omega$-turbulence model was chosen over other turbulence models as it gave more stable results (c.f. [36]). The monoplane (biplane) airfoil was placed 10m (15m) behind the inlet of the virtual wind tunnel with 40m (60m) length and 20m (30m) height.

Discussion of results

The velocity field and pressure coefficient field in Fig. 7 show a smooth flow. For the biplane configuration, the flow speed was higher for the upper wing than for the lower wing, and thus the pressure on the upper surface of the upper wing was lower than that of the lower wing. Therefore, Fig. 8 shows that the share of the forces was not equal: The lift and drag coefficients of the upper wing were higher than the values for the lower wing. However, the total/average lift coefficients of the biplane were almost identical to the values of the monoplane. Only the total/average drag coefficients of the biplane were slightly higher than that of the monoplane, but the difference was less than 10%. Therefore, the assumption made in the previous sections to neglect the aerodynamic interference of the upper and lower wing of the biplane can be confirmed. The stall at a low angle of attack was relatively abrupt, which can be explained by the sharp lower edge of the first wing element. However, this stall occurred

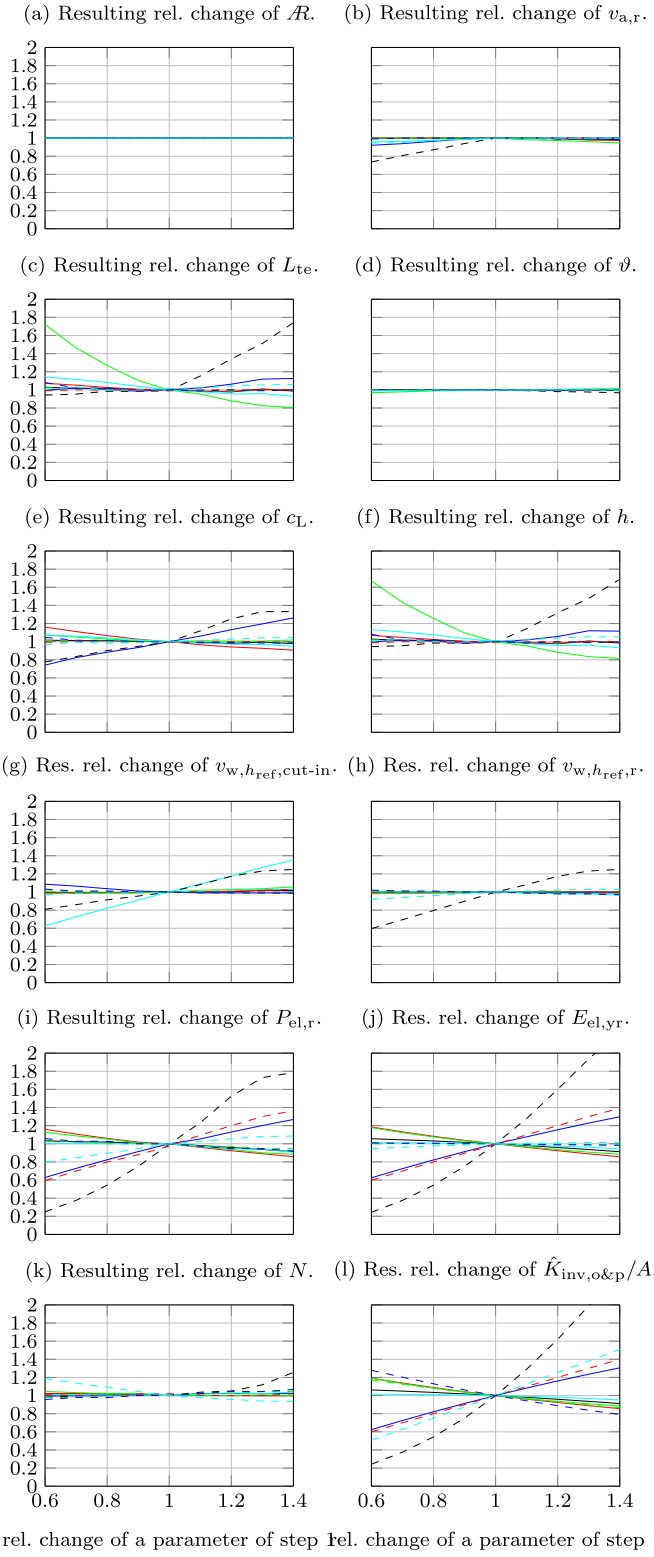

Fig. 6. Relative changes of (a)–(f) optimized parameters and (g)–(l) figures of merit for relative changes of a parameter of step 1, where azimuth φ in (–), drag coefficient slope w.r.t. the lift coefficient squared $c_{D,2}$ in (——), tether increase factor f_{te} in (——), Oswald efficiency factor e in (——), minimum airspeed $v_{a,min}$ in (——), mean wind speed in reference altitude $\bar{v}_{w,h_{ref}}$ in (- - -), efficiency η in (– – ·), operational cost percentage l_{op} in (– – ·), interest rate I in (– – ·), levelized cost of electricity k_{LCOE} in (– – ·).

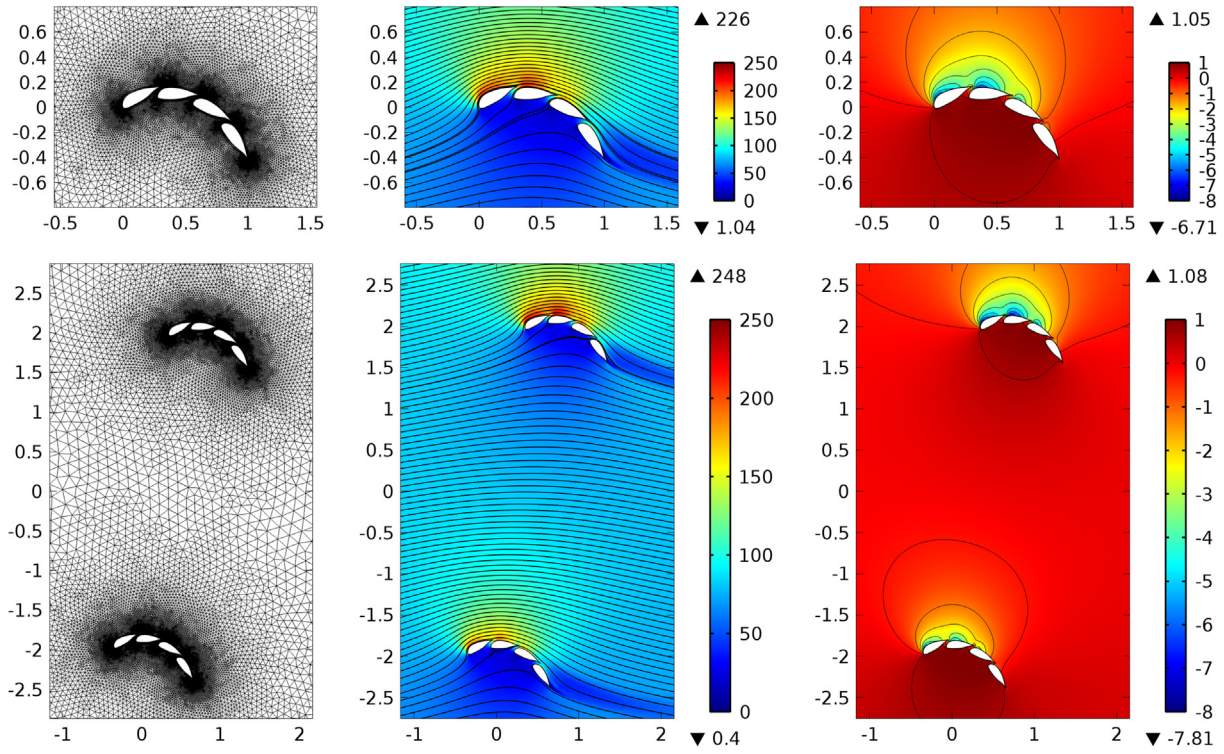

Fig. 7. CFD results for the designed airfoil in monoplane configuration (top) and biplane configuration (bottom): (unstructured) mesh (left), velocity field (middle) and pressure coefficient field (right). All space coordinates are in m and all speed values are in m/s.

at relatively low angles of attack, which are unlikely in normal operation, as the lift shall mainly be controlled by the flaperons. The stall behavior for high angles of attack was very smooth, which is beneficial and can be explained by the gaps between the airfoil elements which create a fast flow on the upper surface of every next airfoil element which in turn generates a low pressure and thus forces a certain attachment of the flow. For reference, the bottom plot of Fig. 8 shows the polar of the simplified model (22) with the parameters of Table 1, with which model and parameters (apart from stalling), used for all computations of the utility-scale system of the previous sections, can be validated.

The total lift coefficient of the proposed airfoil already achieves the optimal lift coefficient in Table 3. However, for a deployment site with higher mean wind speed or for a wing with higher Oswald efficiency, even higher lift coefficients are optimal (cf. Fig. 6). Moreover, the two main purposes of the CFDs were (i) to use reasonable values for $c_{D,0}$ and $c_{D,2}$ for the airfoil polar model (22) and (ii) to justify the assumption that the aerodynamic interference of the biplane wings is negligible. Hence, for an actual drag power kite realization, further airfoil analyses and optimizations are required.

3.6. Proposed planform design of a drag power kite

Fig. 9 shows the proposed planform design of the utility-scale biplane kite with 40m wing span:

The two main wings are as in Fig. 7 (bottom), seen from the side, and are connected through vertical wings with symmetric airfoils. The rotors are attached to the eight outer joints of the vertical wings and the main wings. Therefore, the downwashes of the rotors do not affect the tail, which is crucial particularly during hovering. As the rotors are connected close to the ends of the wings, they can not only actuate a large moment, but can also compensate partly the wing tip vortexes. Moreover, the vertical wings at the wing tips function as winglets and also form a box wing together with the main wings. Therefore, an increased Oswald efficiency factor e could be expected. The kite has a large tail to control the angle of attack and angle of sideslip and to compensate the relatively strong moments imposed by the main wings for changed angles of attack or flaperon angles. Moreover, the tail compensates the moments imposed by the tether, as the tether connection does not coincide with the center of mass. The elevator is behind and above the center of mass and can be fully rotated. Therefore, the elevator can also help to control the pitch during hovering, similar to Makani Power's/Google's kite [37]. The rotors are in front of the main wings and thus disturb and reduce the airflow which leads to a lower lift of these wing sections behind the rotors. However, as the induction factor of the rotors of a drag power kite is rather low (cf. [2, Chap. 28.2.5]) and the affected wing section is rather small, the lift reduction is small. Moreover, as this lift reduction is induced at or close to the wing tips, it could even help to form a more elliptical lift distribution and thus could increase the Oswald efficiency factor e for the considered simple rectangular wings without washout.

The kite's power and tether force are mainly limited by the kite's lift, and the kite's lift is mainly controlled by the flaperons instead of changing the angle of attack. As a reduced lift considerably also reduces the drag, the kite's speed might increase to too high values, cf. (9). To limit/control the airspeed in this case, the drag can be increased through the vertical wings by introducing an angle of sideslip controlled by the rudders, or by air brakes mounted to the vertical wings.

The proposed design can be seen as a merger of Makani Power's/Google's and Joby Energy's design (cf. [6]. with [38]): The

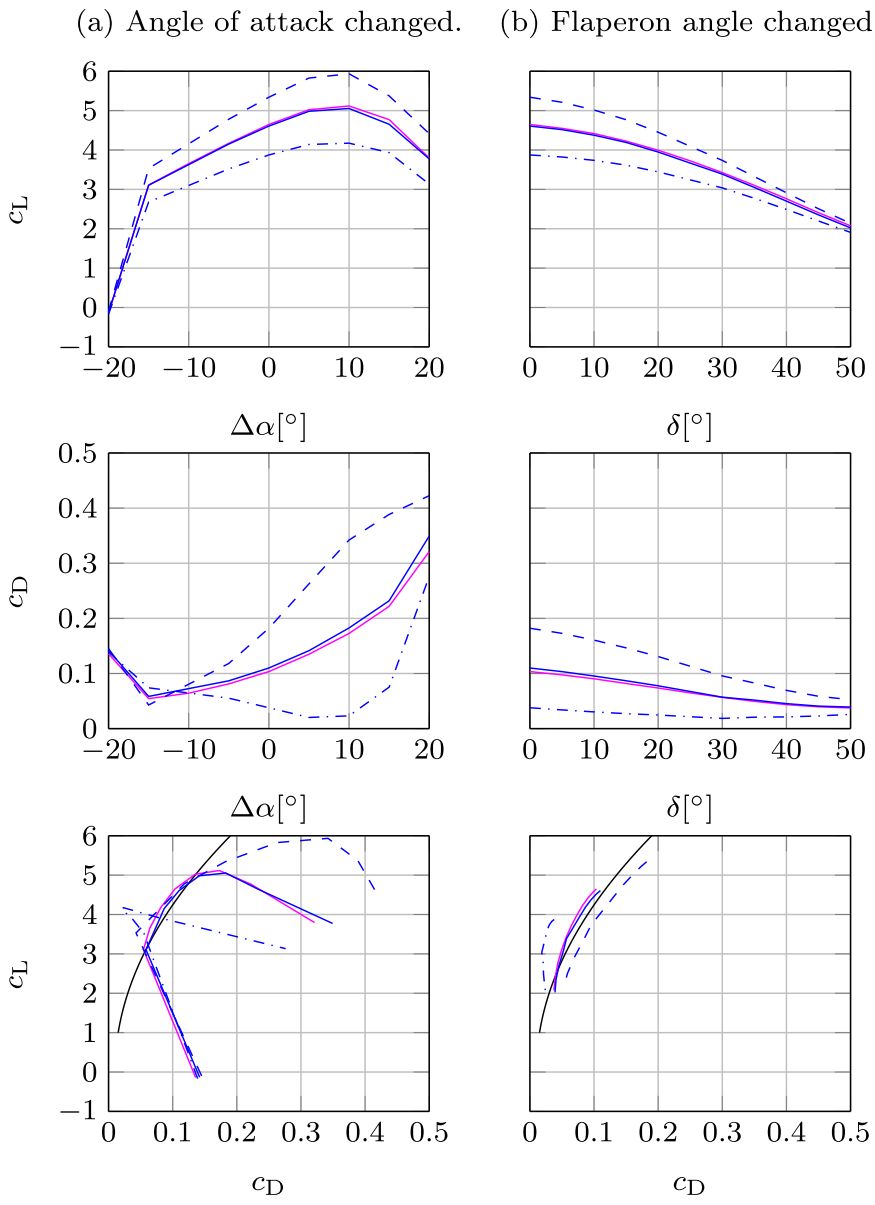

Fig. 8. CFD results of the designed airfoil for changes of the angle of attack $\Delta\alpha$ (a) and changes of the flaperon angle δ (b) (the flaperon is the most right wing element in Fig. 7) with monoplane configuration in magenta and biplane configuration in blue. From top to bottom: lift coefficient as function of $\Delta\alpha$ or δ, respectively; drag coefficient as function of $\Delta\alpha$ or δ, respectively; and polars, i.e. lift coefficient as function of drag coefficient. For the biplane configuration, the upper wing is in dashed (- - -), the lower wing is in dash-dotted (-·-·-), and the total/average is in solid (—). Hereby, the reference chord to compute the coefficients was 1m (cf. Fig. 7). For reference, also the simplified model (22) with the parameters of Table 1 for the biplane is plotted in the bottom polar plot in black solid (—).

differences to Makani Power's/Google's design are the use of more than two elements [39] for a very high-lift multi-element airfoil, and the biplane configuration. The difference to Joby Energy's design [38] is the use of a high-lift multi-element airfoil instead of a reflex airfoil which cannot achieve high lift coefficients, but requires no tail to compensate the aerodynamic moments for changes of angle of attack or flaperon angle.

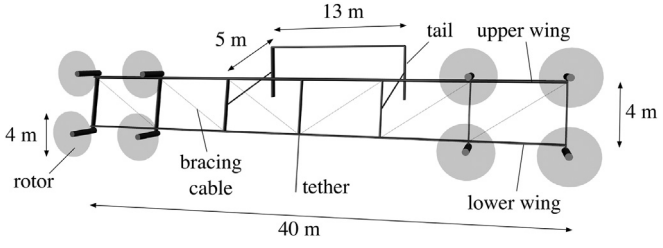

Fig. 9. Proposed utility-scale biplane kite design.

4. Conclusions & outlook

In this study, the Hypothesis was made, that maximizing a drag power kite's lift coefficient to or close to its physically feasible maximum, also maximizes its power, energy yield as well as maximum allowed costs and profit margin. For that, a simplified model from literature was extended and rearranged into a sequence of explicit analytical equations. Numerical results for lift coefficients between one and six proved the hypothesis for four different kite variants. Additionally, the utility-scale kite

variant was optimized with a genetic algorithm with the additional kite power plant parameters, which were fixed to "some" values in the previously mentioned analyses. In all results, a biplane kite with a very high lift coefficient outperformed a monoplane kite. The optimized utility-scale biplane with 40m span and 80m^2 wing area achieved a rated electrical power of ≈4.1MW at a rated wind speed of ≈10m/s. Hence, the expected power density was ≈52kW/m^2. A high-lift multi-element airfoil with four elements was proposed. Through CFD simulations, a maximum lift coefficient of slightly above 5 at a drag coefficient of ≈0.18 was achieved, although the airfoil itself was mainly designed through trail and error. As the main wings of the biplane were separated by several chord lengths, the interference of both wings proved to be negligible. The CFDs also verified the simple aerodynamic model and parameters used in the kite model for the previous analyses (apart from stall). Finally, a planform design of the 40m span utility-scale biplane kite was proposed.

In a future work, the model could be further improved or coupled with more elaborate sub-models: E.g. the CFD could be included in the optimization to optimize simultaneously the kite parameters like the tether length etc. and the airfoil parameters like the gap size etc. However, a drawback of such model improvements could be a considerable increase of the computational load. Another improvement could be the replacement of the tether increase factors by electrical cable models, which could also be used to increase the fidelity of the efficiency estimation. A multibody dynamic model and controllers were already developed by the authors of this study to increase the fidelity of the kite- and tether dynamics which show similar results for the power estimation, but further work is required. Moreover, basic stiffness and hovering tests with a small biplane demonstrator were already performed successfully, despite the fact that the center of mass does not coincide with the tether connection, which leads to moments induced by the tether. A validation of the proposed concept with a fully functional demonstrator is currently planned by the authors. With the help of demonstrators, also precise cost models of the system parts (airframe, ground station etc.) could become available, with which the optimization cost function could be changed to maximize solely the profit margin.

Acknowledgment

This study received funding from "Bund der Freunde der TU München e.V." and from the European Union's Horizon 2020 research and innovation programme under the Marie Skłodowska-Curie grant agreement No 642682.

Appendix. Power equation further elaborated analytically

An important figure of merit of a kite design is its (rated) power. In the following, the power equation (15) is further elaborated analytically: Inserting all equations of the aerodynamic coefficients (8), (17), (19)–(21), (29), (31)–(33), the power is given by

$$\begin{aligned}
P_\mathrm{a}^* &= \frac{2}{27}\rho\cos^3(\varphi)\cos^3(\vartheta)v_\mathrm{w}^3 A\frac{C_\mathrm{L}^3}{C_\mathrm{D,eq}^2}\\
&= \frac{2}{27}\rho\cos^3(\varphi)\cos^3(\vartheta)v_\mathrm{w}^3 A\\
&\quad\frac{\left(\frac{c_\mathrm{L}}{1+\frac{2}{AR}}\right)^3}{\left(\underbrace{c_\mathrm{D}+C_\mathrm{D,k,o}}_{=:\tilde{c}_\mathrm{D}}+\frac{C_\mathrm{L}^2}{\pi e AR}+\frac{1}{3}\frac{d_\mathrm{te}L_\mathrm{te}}{A}c_\mathrm{D,te}\right)^2}\\
&= \frac{2}{27}\rho\cos^3(\varphi)\cos^3(\vartheta)v_\mathrm{w}^3 A\\
&\quad\frac{\left(\frac{c_\mathrm{L}}{1+\frac{2}{AR}}\right)^3}{\left[\tilde{c}_\mathrm{D}+\frac{\left(\frac{c_\mathrm{L}}{1+\frac{2}{AR}}\right)^2}{\pi e AR}+\frac{1}{3}\frac{\left(2\sqrt{\frac{S_\mathrm{te}F_\mathrm{te,r}}{\sigma_\mathrm{te}\pi}}f_\mathrm{te}+\Delta_\mathrm{te}\right)L_\mathrm{te}}{A}c_\mathrm{D,te}\right]^2}\\
&= \frac{2}{27}\rho\cos^3(\varphi)\cos^3(\vartheta)v_\mathrm{w}^3 A\\
&\quad\frac{\left(\frac{c_\mathrm{L}}{1+\frac{2}{AR}}\right)^3}{\left[\tilde{c}_\mathrm{D}+\frac{\left(\frac{c_\mathrm{L}}{1+\frac{2}{AR}}\right)^2}{\pi e AR}+\frac{1}{3}\frac{\left(2\sqrt{\frac{S_\mathrm{te}\frac{1}{2}\rho v_\mathrm{a,r}^2 A C_\mathrm{L,r}}{\sigma_\mathrm{te}\pi}}f_\mathrm{te}+\Delta_\mathrm{te}\right)L_\mathrm{te}}{A}c_\mathrm{D,te}\right]^2}\\
&= \frac{2}{27}\rho\cos^3(\varphi)\cos^3(\vartheta)v_\mathrm{w}^3 A\\
&\quad\frac{\left(\frac{c_\mathrm{L}}{1+\frac{2}{AR}}\right)^3}{\left[\tilde{c}_\mathrm{D}+\frac{\left(\frac{c_\mathrm{L}}{1+\frac{2}{AR}}\right)^2}{\pi e AR}+\frac{1}{3}\frac{\left(2\sqrt{\frac{S_\mathrm{te}\frac{1}{2}\rho v_\mathrm{a,r}^2 A\frac{c_\mathrm{L}}{1+\frac{2}{AR}}}{\sigma_\mathrm{te}\pi}}f_\mathrm{te}+\Delta_\mathrm{te}\right)L_\mathrm{te}}{A}c_\mathrm{D,te}\right]^2}.
\end{aligned} \tag{73}$$

where parasitic drag coefficient and the drag coefficient of other parts is summarized by

$$\tilde{c}_\mathrm{D} := c_\mathrm{D} + C_\mathrm{D,k,o}. \tag{74}$$

For $\Delta_\mathrm{te} = 0$ (without loss of generality as $f_\mathrm{te} \neq 0$) this equation can be written as

$$P_\mathrm{a}^* = \frac{k_1 c_\mathrm{L}^3}{\left[\tilde{c}_\mathrm{D}+\frac{\left(\frac{c_\mathrm{L}}{1+\frac{2}{AR}}\right)^2}{\pi e AR}+k_2\sqrt{c_\mathrm{L}}\right]^2}. \tag{75}$$

where

$$k_1 = \frac{2}{27}\rho\cos^3(\varphi)\cos^3(\vartheta)v_\mathrm{w}^3 A\left(\frac{1}{1+\frac{2}{AR}}\right)^3. \tag{76}$$

and

$$k_2 = \frac{1}{3}\frac{\left(2\sqrt{\frac{S_{te}\frac{1}{2}\rho v_{a,r}^2 A\frac{1}{1+\frac{2}{\mathcal{AR}}}}{\sigma_{te}\pi}}f_{te}\right)L_{te}}{A}c_{D,te}. \tag{77}$$

Consider three extreme cases:

Case 1: The tether drag is dominant, i.e. $k_2\sqrt{c_L} \gg \tilde{c}_D + \left[c_L/(1+\frac{2}{\mathcal{AR}})\right]^2/(\pi e\mathcal{AR})$, so the power can be expressed by

$$P_a^* \approx \frac{k_1 c_L^3}{(k_2\sqrt{c_L})^2} = \frac{k_1}{k_2^2}c_L^2 \quad \sim c_L^2. \tag{78}$$

Case 2: The kite's parasitic drag is dominant, i.e. $\tilde{c}_D \gg \left[c_L/(1+\frac{2}{\mathcal{AR}})\right]^2/(\pi e\mathcal{AR}) + k_2\sqrt{c_L}$, so the power can be expressed by

$$P_a^* \approx \frac{k_1 c_L^3}{\tilde{c}_D^2} \quad \sim \frac{c_L^3}{\tilde{c}_D^2}. \tag{79}$$

Case 3: The kite's induced drag is dominant, i.e. $\left[c_L/(1+\frac{2}{\mathcal{AR}})\right]^2/(\pi e\mathcal{AR}) \gg \tilde{c}_D + k_2\sqrt{c_L}$, so the power can be expressed by

$$P_a^* \approx \frac{k_1 c_L^3}{\left[\frac{\left(\frac{c_L}{1+\frac{2}{\mathcal{AR}}}\right)^2}{\pi e\mathcal{AR}}\right]^2} = \frac{k_1}{\frac{\left(\frac{1}{1+\frac{2}{\mathcal{AR}}}\right)^4}{(\pi e\mathcal{AR})^2}}\frac{1}{c_L}. \tag{80}$$

Consequently, the following conclusions can be drawn: If the tether drag is dominant (case 1), the power increases with the square of the main wing airfoil's lift coefficient. Consequently, a high-lift (multi-element) airfoil should be used. If the parasitic drag is dominant (case 2), the ratio $c_L^3/\tilde{c}_D^2$ should be maximized, which is similar to a maximization of c_L for usual airfoils. If the induced drag is dominant (case 3), the aspect ratio might better be increased. Note that a high aspect ratio is beneficial in all cases.

References

[1] M.L. Loyd, Crosswind kite power, J. Energy 4 (3) (1980) 106–111, https://doi.org/10.2514/3.48021.

[2] U. Ahrens, M. Diehl, R. Schmehl (Eds.), Airborne Wind Energy, Springer, Berlin Heidelberg, 2013, https://doi.org/10.1007/978-3-642-39965-7.

[3] L. Fagiano, M. Milanese, Airborne wind energy: an overview, in: Proceedings of the 2012 American Control Conference, IEEE, Montréal, Canada, 2012, pp. 3132–3143.

[4] A. Cherubini, A. Papini, R. Vertechy, M. Fontana, Airborne wind energy systems: a review of the technologies, Renew. Sustain. Energy Rev. 51 (2015) 1461–1476, https://doi.org/10.1016/j.rser.2015.07.053.

[5] J.W. Kolar, T. Friedli, F. Krismer, A. Looser, M. Schweizer, P. Steimer, J. Bevirt, Conceptualization and multi-objective optimization of the electric system of an airborne wind turbine, in: 2011 IEEE International Symposium on Industrial Electronics (ISIE), 2011, pp. 32–55, https://doi.org/10.1109/ISIE.2011.5984131.

[6] Makani Power/Google. [link]. URL https://www.google.com/makani/.

[7] D. V. Lind, Developing a 600 kW Airborne Wind Turbine. URL http://awec2015.tudelft.nl/presentations.html.

[8] Makani, Makani's first commercial-scale energy kite. URL https://www.youtube.com/watch?v=An8vtD1FDqs.

[9] M. Canale, L. Fagiano, M. Ippolito, M. Milanese, Control of tethered airfoils for a new class of wind energy generator, in: 2006 45th IEEE Conference on Decision and Control, 2006, pp. 4020–4026, https://doi.org/10.1109/CDC.2006.376775.

[10] M. Zanon, S. Gros, J. Andersson, M. Diehl, Airborne wind energy based on dual airfoils, IEEE Trans. Control Syst. Technol. 21 (4) (2013) 1215–1222, https://doi.org/10.1109/TCST.2013.2257781.

[11] A. Bormann, Global Economy of Airborne Wind Energy and our Path Towards a Market-Ready Technology. URL http://awec2015.tudelft.nl/presentations.html.

[12] A. Venturato, Analisi fluidodinamica del profilo alare clark-y ed ottimizzazione multi-obbiettivo tramite algoritmo genetico, Master's thesis, Università degli studi di Padova, 2013, http://tesi.cab.unipd.it/44507/1/Tesi_Venturato_Andrea_607493.pdf.

[13] R. J. Coenen, S. Drenth, T. Smits, M. L. W. Veraart, Design of a Lightweight and Durable Kite for Pumping Kite Power Generation. URL http://www.awec2015.com/images/posters/AWEC10_Coenen-poster.pdf.

[14] J. Heilmann, Technical and Economic Potential of Airborne Wind Energy, Master thesis, Utrecht University, 2012, http://dspace.library.uu.nl/handle/1874/258716.

[15] C. Grete, Optimization, Scaling and Economics of Pumping Kite Power Systems, Master thesis, Delft University of Technology, 2014. https://repository.tudelft.nl/islandora/object/uuid%3Ab980aab7-f346-4030-97a3-a3cde13a51d6?collection=education.

[16] D. Vander Lind, Airfoil for a flying wind turbine, US Patent 9,709,026 (Jul. 18 2017).

[17] L. Fagiano, Control of Tethered Airfoils for High-altitude Wind Energy Generation, Ph.D. thesis, Politecnico di Torino, 2009, http://lorenzofagiano.altervista.org/docs/PhD_thesis_Fagiano_Final.pdf.

[18] A.M.O. Smith, High-lift aerodynamics, J. Aircr. 12 (6) (1975) 501–530, https://doi.org/10.2514/3.59830. https://doi.org/10.2514/3.59830.

[19] L. Fagiano, A. Zgraggen, M. Morari, M. Khammash, Automatic crosswind flight of tethered wings for airborne wind energy: modeling, control design, and experimental results, IEEE Trans. Control Syst. Technol. 22 (4) (2014) 1433–1447, https://doi.org/10.1109/TCST.2013.2279592.

[20] J. Katz, A. Plotkin, Low-speed Aerodynamics, Cambridge Aerospace Series, Cambridge University Press, 2001.

[21] B. Houska, M. Diehl, Optimal control for power generating kites, in: Proceedings of the 9th European Control Conference, Kos, Greece, 2007, pp. 3560–3567. http://www.kuleuven.be/optec/files/Houska2007.pdf.

[22] I. Argatov, P. Rautakorpi, R. Silvennoinen, Estimation of the mechanical energy output of the kite wind generator, Renew. Energy 34 (6) (2009) 1525–1532 http://www.sciencedirect.com/science/article/pii/S096014810800400X, http://doi.org/10.1016/j.renene.2008.11.001.

[23] I. Argatov, P. Rautakorpi, R. Silvennoinen, Apparent wind load effects on the tether of a kite power generator, J. Wind Eng. Ind. Aerodynamics 99 (10) (2011) 1079–1088. http://doi.org/10.1016/j.jweia.2011.07.010. http://www.sciencedirect.com/science/article/pii/S0167610511001449.

[24] T. Burton, N. Jenkins, D. Sharpe, E. Bossanyi, Wind Energy Handbook, Wiley, 2011.

[25] V. Quaschning, Regenerative Energiesysteme: Technologie - Berechnung - Simulation, Hanser, 2007.

[26] J. Schlabbach, Elektroenergieversorgung: Betriebsmittel, Netze, Kennzahlen und Auswirkungen der elektrischen Energieversorgung, VDE-Verlag, 2009.

[27] N. Boccard, Capacity Factor of Wind Power: Realized Values Vs. Estimates, 2009, https://doi.org/10.2139/ssrn.1285435. https://ssrn.com/abstract=1285435.

[28] W. Short, D. Packey, T. Holt, A Manual for the Economic Evaluation of Energy Efficiency and Renewable Energy Technologies, National Renewable Energy Laboratory (NREL), 1995.

[29] Makani Power, Inc., Response to the federal aviation authority, Docket No.: FAA-2011-1279; Notice No. 11-07; Notification for Airborne Wind Energy Systems (AWES). URL http://www.energykitesystems.net/FAA/FAAfromMakani.pdf.

[30] Erneuerbare-Energien-Gesetz vom 25. Oktober 2008 (BGBl. I S. 2074), das durch Artikel 1 des Gesetzes vom 17. August 2012 (BGBl. I S. 1754) geändert worden ist, Anlage 3, Absatz 4. [link]. URL https://www.clearingstelle-eeg.de/files/EEG2012_juris_120817.pdf.

[31] Hobbyking.com. [link]. URL https://hobbyking.com/en_us/turnigy-rotomax-100cc-size-brushless-outrunner-motor.html.

[32] Wind Energy Online Reader. [link]. URL http://mstudioblackboard.tudelft.nl/duwind/Wind%20energy%20online%20reader/Static_pages/annual_energy.htm.

[33] N. Hansen, The CMA evolution strategy: A tutorial, CoRR abs/1604.00772. URL http://arxiv.org/abs/1604.00772.

[34] F. Bauer, C.M. Hackl, K. Smedley, R.M. Kennel, Crosswind kite power with tower, in: R. Schmehl (Ed.), Airborne Wind Energy, Springer, Singapore, 2018.

[35] Comsol, Comsol 4.4, CFD Module User's Guide, 2013.

[36] M. Murayama, Z. Lei, J. Mukai, K. Yamamoto, CFD validation for high-lift devices: three-element airfoil, Trans. Jpn. Soc. Aeronautical Space Sci. 49 (163) (2006) 40–48, https://doi.org/10.2322/tjsass.49.40.

[37] D. Vander Lind, Planform configuration for stability of a powered kite and a system and method for use of same, US Patent 8,800,931 (Aug. 12 2014).

[38] Joby Energy. [link]. URL http://jobyenergy.com/.

[39] D. Vander Lind, Kite configuration and flight strategy for flight in high wind speeds, US Patent App. 13/288,527 (May 3 2012).